

Free energy profile along a discretized reaction path via the hyperplane constraint force and torque

Konstantin N. Kudin and Roberto Car

Department of Chemistry and Princeton Institute for Science and Technology of Materials (PRISM), Princeton University, Princeton, New Jersey 08544

(Received 1 December 2004; accepted 26 January 2005; published online 21 March 2005)

By employing mechanical work analogies, we derive a convenient computational approach for evaluation of the free energy profile (FEP) along some discretized path defined as a sequence of hyperplanes. A hyperplane is fully specified by any of its point and a tangent vector. The FEP is obtained as an integral of two components. The translational component of the free energy is computed by integrating the hyperplane constraint force. The rotational component is evaluated via the hyperplane torque. Both ingredients—the constraint force and the hyperplane torque—are evaluated on each hyperplane independently. The integration procedure utilizes a set of reference points defining a point of rotation on each hyperplane, and these points can be chosen before or after the sampling takes place. A shift in the reference points redistributes the FEP contributions between the translational and rotational components. For systems where the FEP is dominated by the potential energy differences, reference points residing on the minimum energy path present a natural choice. We demonstrate the validity of our approach on two examples, a simple two-dimensional (2D) potential, and a seven-atom Lennard-Jones cluster. In each case, we compare the numerical FEP with the harmonic approximation estimates. Our results for the 2D potential are also verified by the data available in the literature. In both cases, the rotational component of the FEP represents a sizable contribution to the total FEP, so ignoring it would yield clearly incorrect results. © 2005 American Institute of Physics. [DOI: 10.1063/1.1874832]

I. INTRODUCTION

Evaluation of reaction free energies via configuration sampling is one of the widely utilized techniques in simulations of chemical and biochemical systems. The knowledge of free energy differences for reactants, products, and transition states allows one to predict the direction of chemical reactions as well as estimate their reaction rates.¹

Of specific interest to us are sampling approaches that allow to compute free energy profiles (FEP) with reliable and thus computationally expensive interatomic potentials such as *ab initio* molecular dynamics.² The time scales accessible with such potentials tend to be rather short, so chemical reaction events with high activation energies are “rare” and unlikely to happen during the simulation time. To achieve sufficient sampling around a likely path one can utilize constraints of some sort to drive the system from the reactant to the product region.³ This procedure requires some *a priori* choice of a reaction coordinate along which the system is forced to move.

In such cases, a good choice of the reaction coordinate is critical for the success of the whole procedure. A reaction coordinate can be considered to be “good” when one with high probability finds the system to be in the reactant region below a certain reaction coordinate value, and in the product region above it.⁴ After computing the free energy profile and specifying the dividing surface between the reactants and products at the maximum of the FEP, one can launch trajectories in order to make sure that indeed the reaction coordinate is a good one.^{5,6} In commonly found situations, the re-

actants and products are connected via a single low energy tube, so the neighborhood of the minimum energy path is a good representation of the configuration space region through which pass almost all reactive trajectories. Then, if one can manage to represent such a good path via a single internal coordinate, the FEP evaluation is especially straightforward via the force of constraint in molecular dynamics simulations (MD) as discussed by den Otter and Briels,⁷ and by Sprik and Ciccotti.⁸

Here, by using mechanical work analogies, we aim to derive a physically transparent and computationally convenient approach for evaluating the FEP along a *discretized* reaction path. A path is specified via a sequence of hyperplanes which could be obtained by any of the methods such as the intrinsic reaction path,⁹ nudged elastic band,¹⁰ or string method.^{11,12} We should note that the FEP integration for numerical paths utilizing translational and rotational terms have already been discussed in the literature by Jonsson and co-workers^{13,14} and Neria *et al.*¹⁵ Others have also attempted to compute free energies along such paths.^{16–18} We believe that the advantage of our formulas compared to the earlier ones^{13–15} is that we clearly express the FEP as an integral of two simple averages evaluated on each hyperplane independently—the force of the constraint representing the work of the hyperplane translation and the torque accounting for the hyperplane rotation. Our expressions also highlight the fact that the point specifying a given hyperplane is separable from the averages, and can be set before or after the averages are computed. This point can be

the configuration residing on the initial minimum energy path, the thermally averaged configuration in the hyperplane calculated during the simulation, or some other point. We show how different choices of the reference points redistribute the work between translational and rotational contributions. For both numerical example presented, we validate the FEP computed via the constrained MD by comparing it to the free energy differences obtained via the harmonic approximation.

II. APPROACH

A. Free energy change between two hyperplanes

Let us consider some system with M Cartesian coordinates and multiple local energy minima in this M -dimensional space. A discretized reaction path connecting two minima will be represented as a sequence of configurations $\tilde{\mathbf{R}}_i$ specifying a point on each configurational hyperplane i , and normalized tangents \mathbf{n}_i ($|\mathbf{n}_i|=1$). Such a set of $\tilde{\mathbf{R}}_i$ and \mathbf{n}_i could be obtained, for example, via the nudged elastic band method¹⁰ or the string method,¹¹ and even simple linear interpolation between the initial and final states of the system¹⁴ would also give a valid albeit possibly suboptimal path.

To confine the system to a given hyperplane $(\tilde{\mathbf{R}}_i, \mathbf{n}_i)$ one applies the constraint

$$[\mathbf{R}_i(t) - \tilde{\mathbf{R}}_i] \cdot \mathbf{n}_i = 0. \quad (1)$$

The dimensionality of the subspace specified by such a hyperplane is $(M-1)$.

The free energy A of a given hyperplane at temperature T can be written as

$$A(\tilde{\mathbf{R}}_i, \mathbf{n}_i) = -k_B T \ln Q(\tilde{\mathbf{R}}_i, \mathbf{n}_i), \quad (2)$$

where k_B is Boltzmann's constant and $Q(\tilde{\mathbf{R}}_i, \mathbf{n}_i)$ is the partition function. The probability to find the system at a given point of such $(\tilde{\mathbf{R}}_i, \mathbf{n}_i)$ hyperplane is determined by the available kinetic energy, which is the function of temperature T . Suppose that now the tangent is arbitrarily rotated from \mathbf{n}_i to \mathbf{n}'_i in the full M -dimensional space. The hyperplane $(\tilde{\mathbf{R}}_i, \mathbf{n}'_i)$ now specifies a different $(M-1)$ subspace compared to the earlier hyperplane $(\tilde{\mathbf{R}}_i, \mathbf{n}_i)$, and thus will have a different partition function Q . In the following, we refer to such a change in the hyperplane tangent as "rotation." The free energy change (work) due to the tangent rotation is in general non-zero

$$W_{i',i}^{ROT} = k_B T [\ln Q(\tilde{\mathbf{R}}_i, \mathbf{n}'_i) - \ln Q(\tilde{\mathbf{R}}_i, \mathbf{n}_i)] \neq 0. \quad (3)$$

The free energy difference for two consecutive hyperplanes is

$$W_{i \rightarrow i+1} = A(\tilde{\mathbf{R}}_{i+1}, \mathbf{n}_{i+1}) - A(\tilde{\mathbf{R}}_i, \mathbf{n}_i). \quad (4)$$

When both hyperplanes i and $i+1$ have the same tangent $\mathbf{n}_{i+1} = \mathbf{n}_i$ (i.e., a simple linear constraint) the work $W_{i \rightarrow i+1}$ can be obtained as a straightforward integral of the constraint force over the coordinate change.^{7,8} This is because we are dealing with just a simple linear reaction coordinate and the

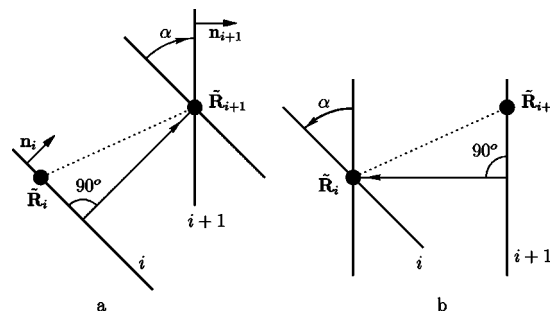


FIG. 1. Transformation of hyperplanes in the forward and reverse directions.

Jacobian of such a transformation is trivial ($|J|=1$), so all complicated factors go away. The constraint force is just the ensemble averaged force acting on the hyperplane i along the tangent, defined as

$$\langle F_i^{\parallel} \rangle = \langle \mathbf{F}_i \cdot \mathbf{n}_i \rangle. \quad (5)$$

Integrating $\langle F_i^{\parallel} \rangle$ force along the path would be sufficient for getting the entire FEP if there was no change in the tangent orientation. However, in general, the tangents do rotate from hyperplane to hyperplane.

Thus we also need a preferably simple way to compute the rotational contribution. The transformation of hyperplane i to hyperplane $i+1$ can be viewed as a sequence of two steps. First, hyperplane i is translated until one of its points coincides with $\tilde{\mathbf{R}}_{i+1}$, and then it is rotated around point $\tilde{\mathbf{R}}_{i+1}$ in order to align tangents \mathbf{n}_i and \mathbf{n}_{i+1} [Fig. 1(a)].¹⁵ Naturally, one could just as well carry out the transformations in the opposite direction [Fig. 1(b)].

So the total work required to carry out the forward transformation could be split into two components

$$W_{i \rightarrow i+1} = W_{i \rightarrow i+1}^{TR} + W_{i' \rightarrow i+1}^{ROT}. \quad (6)$$

As mentioned earlier, the translational work $W_{i \rightarrow i+1}^{TR}$ is evaluated as force times the displacement

$$W_{i \rightarrow i+1}^{TR} = ([\tilde{\mathbf{R}}_{i+1} - \tilde{\mathbf{R}}_i] \cdot \mathbf{n}_i) \langle F_i^{\parallel} \rangle, \quad (7)$$

where $[\tilde{\mathbf{R}}_{i+1} - \tilde{\mathbf{R}}_i] \cdot \mathbf{n}_i$ is the translation distance [Fig. 1(a)]. One could notice a strong analogy with the mechanical work, similarly defined as force times the displacement. We want to emphasize that the displacement of hyperplane i implies not just a translation of a single configuration $\tilde{\mathbf{R}}_i$, but rather of the whole potentially accessible $(M-1)$ -dimensional subspace $(\tilde{\mathbf{R}}_i, \mathbf{n}_i)$ to a new location in the full M -dimensional space. The work required represents the change in the free energy defined in Eq. (2).

B. Rotational work

Continuing to borrow from mechanics, the work due to hyperplane rotation $[(\tilde{\mathbf{R}}_i, \mathbf{n}_i) \rightarrow (\tilde{\mathbf{R}}_i, \mathbf{n}'_i)]$ is the product of the torque and rotational angle α . Instead of computing the work $W_{i' \rightarrow i+1}^{ROT}$ needed to rotate translated hyperplane i at the intermediate location [Fig. 1(a)], we choose to evaluate the negative of the work $W_{i+1 \rightarrow i'}^{ROT}$ needed to rotate hyperplane $i+1$ to

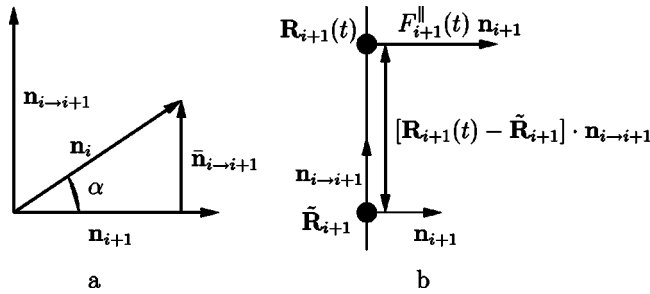


FIG. 2. Hyperplane rotations and the associated direction and torque.

match translated hyperplane i . This is because the torque on unmodified hyperplane $i+1$ is known exactly since this is where the sampling takes place. In the following we refer to this rotational work as $W_{i+1,i}^{ROT} = -W_{i+1 \rightarrow i'}^{ROT} = W_{i' \rightarrow i+1}^{ROT}$. Note that to understand all the physics involved in rotating hyperplanes it is already sufficient to consider one-dimensional (1D) “hyperplanes” (lines) in a “full” 2D space, such as what is shown in Fig. 1. The rotation of hyperplane $i+1$ occurs around point $\tilde{\mathbf{R}}_{i+1}$ [Fig. 1(a)] in a 2D subspace spanned by vectors \mathbf{n}_i and \mathbf{n}_{i+1} . We will choose as the orthonormal basis in this 2D subspace vectors \mathbf{n}_{i+1} and the normalized component of \mathbf{n}_i orthogonal to \mathbf{n}_{i+1} [Fig. 2(a)]

$$\mathbf{n}_{i \rightarrow i+1} = \frac{\mathbf{n}_i - (\mathbf{n}_i \cdot \mathbf{n}_{i+1})\mathbf{n}_{i+1}}{|\mathbf{n}_i - (\mathbf{n}_i \cdot \mathbf{n}_{i+1})\mathbf{n}_{i+1}|} = \frac{\bar{\mathbf{n}}_{i \rightarrow i+1}}{|\bar{\mathbf{n}}_{i \rightarrow i+1}|}. \quad (8)$$

In such a basis, vector \mathbf{n}_i can be represented as

$$\mathbf{n}_i = \mathbf{n}_{i+1} \cos(\alpha) + \mathbf{n}_{i \rightarrow i+1} \sin(\alpha), \quad (9)$$

where $\alpha = \arccos(\mathbf{n}_i \cdot \mathbf{n}_{i+1})$. By construction, angle α is such that $\sin(\alpha) \geq 0$ [Fig. 2(a)]. Then the norm of the difference vector $\bar{\mathbf{n}}_{i \rightarrow i+1}$ is

$$|\bar{\mathbf{n}}_{i \rightarrow i+1}| = |\mathbf{n}_i - (\mathbf{n}_i \cdot \mathbf{n}_{i+1})\mathbf{n}_{i+1}| = \sin(\alpha). \quad (10)$$

The fact that $|\bar{\mathbf{n}}_{i \rightarrow i+1}| = \sin(\alpha)$ will help us to simplify the situation when α is close to or is zero. We do not use the vector product expression for the torque from mechanics since in general the entire configuration space has a number of dimensions different from three. The instantaneous scalar torque, on the other hand, can always be defined as

$$\tau_{i+1,i}(t) = F_{i+1}^{\parallel}(t) ([\mathbf{R}_{i+1}(t) - \tilde{\mathbf{R}}_{i+1}] \cdot \mathbf{n}_{i \rightarrow i+1}). \quad (11)$$

The expression $([\mathbf{R}_{i+1}(t) - \tilde{\mathbf{R}}_{i+1}] \cdot \mathbf{n}_{i \rightarrow i+1})$ gives the arm length by projecting the difference between current position $\mathbf{R}_{i+1}(t)$ in the hyperplane and the point of rotation $\tilde{\mathbf{R}}_{i+1}$ onto the vector $\mathbf{n}_{i \rightarrow i+1}$ orthogonal to the force in the 2D plane [Fig 2(b)]. The scalar product specifying the arm length is either positive or negative depending on location of the point $\mathbf{R}_{i+1}(t)$ with respect to point $\tilde{\mathbf{R}}_{i+1}$ [above or below point $\tilde{\mathbf{R}}_{i+1}$ in Fig. 2(b)]. The torque average is

$$\begin{aligned} \langle \tau_{i+1,i} \rangle &= \langle F_{i+1}^{\parallel} ([\mathbf{R}_{i+1} - \tilde{\mathbf{R}}_{i+1}] \cdot \mathbf{n}_{i \rightarrow i+1}) \rangle \\ &= (\langle F_{i+1}^{\parallel} \mathbf{R}_{i+1} \rangle - \langle F_{i+1}^{\parallel} \tilde{\mathbf{R}}_{i+1} \rangle) \cdot \mathbf{n}_{i \rightarrow i+1}. \end{aligned} \quad (12)$$

The notable feature of the last expression is the separation of

constants $\tilde{\mathbf{R}}_{i+1}$ and $\mathbf{n}_{i \rightarrow i+1}$ from the averages $\langle \cdots \rangle$. The rotational work $W_{i+1,i}^{ROT}$ is then

$$W_{i+1,i}^{ROT} = \alpha (\langle F_{i+1}^{\parallel} \mathbf{R}_{i+1} \rangle - \langle F_{i+1}^{\parallel} \tilde{\mathbf{R}}_{i+1} \rangle) \cdot \mathbf{n}_{i \rightarrow i+1}. \quad (13)$$

In the limit of small angles α between \mathbf{n}_i and \mathbf{n}_{i+1} one can use the expression $\sin(\alpha) \approx \alpha$ and rewrite $W_{i+1,i}^{ROT}$ [Eq. (13)] as

$$\begin{aligned} \lim_{\alpha \rightarrow 0} W_{i+1,i}^{ROT} &= \alpha (\langle F_{i+1}^{\parallel} \mathbf{R}_{i+1} \rangle - \langle F_{i+1}^{\parallel} \tilde{\mathbf{R}}_{i+1} \rangle) \cdot \frac{\bar{\mathbf{n}}_{i \rightarrow i+1}}{\sin(\alpha)} \\ &= (\langle F_{i+1}^{\parallel} \mathbf{R}_{i+1} \rangle - \langle F_{i+1}^{\parallel} \tilde{\mathbf{R}}_{i+1} \rangle) \cdot \bar{\mathbf{n}}_{i \rightarrow i+1}. \end{aligned} \quad (14)$$

Equation (14) is applicable even for parallel tangents when $\alpha=0$, in which case $W_{i+1,i}^{ROT}$ is naturally also zero.

It is also instructive to consider the differential form of the expressions for work $W_{i \rightarrow i+1}$. In such a case we will assume that the tangent \mathbf{n}_i is evolving continuously along the segment between planes i and $i+1$, and the segment is parametrized by variable s . This is the approach discussed by Jonsson and co-workers.^{13,14} The differential of the tangent for a given change in the path ds is $[(\partial \mathbf{n}_i / \partial s) ds]$. We note that $\partial \mathbf{n}_i / \partial s$ has the direction opposite to our finite difference vector $\bar{\mathbf{n}}_{i \rightarrow i+1}$ [see Fig. 2(a)], leading to the flip of the sign in the following expression. Then for an instantaneous configuration $\mathbf{R}_i(t)$ the differential of the total work is

$$dW_i(t) = F_i^{\parallel}(t) \left(1 - [\mathbf{R}_i(t) - \tilde{\mathbf{R}}_i] \cdot \frac{\partial \mathbf{n}_i}{\partial s} \right) ds. \quad (15)$$

This work differential is identical to the one given in Refs. 13 and 14.

One can also compute work in the opposite direction for transforming hyperplane $i+1$ into i . In this case, hyperplane $i+1$ is translated toward hyperplane i , and then rotated [Fig. 1(b)]. The expression for such reverse work can be obtained by simply swapping the indices i and $i+1$ in Eq. (6). In general, $W_{i+1 \rightarrow i} = -W_{i \rightarrow i+1}$. However, under the numerical computations the equality is not strictly true, so we will use the average for the purpose of computing the total work,

$$\bar{W}_{i \rightarrow i+1} = [W_{i \rightarrow i+1} - W_{i+1 \rightarrow i}] / 2. \quad (16)$$

We would like to emphasize the fact that during configuration sampling one only needs to compute two rather straightforward averages, the tangent force $\langle F_i^{\parallel} \rangle$, and the average of coordinates weighted by the tangent force $\langle F_i^{\parallel} \mathbf{R}_i \rangle$. This second intermediate will be used for torque evaluation as per Eq. (12).

The point $\tilde{\mathbf{R}}_i$ defining the hyperplane does not appear explicitly in the averages, although, it did define the neighborhood where the sampling started. There is also no coupling between the neighboring hyperplanes in the averages, in contrast to the approach by Neria *et al.*¹⁵ If higher numerical accuracy is desired, additional hyperplanes could be generated by linear interpolation and inserted anywhere along the path, and then extra sampling would only need to be done on these added hyperplanes. The reference points $\tilde{\mathbf{R}}_i$ can be set either before or after the averages are computed, which is quite convenient.

C. Shift in reference points $\tilde{\mathbf{R}}_i$

Now we take a look at what happens when the reference points are shifted. The translational part $W_{i \rightarrow i+1}^{TR}$ changes in the following way:

$$W_{i \rightarrow i+1}^{TR}(\tilde{\mathbf{R}}_i + \Delta\tilde{\mathbf{R}}_i, \tilde{\mathbf{R}}_{i+1}) - W_{i \rightarrow i+1}^{TR}(\tilde{\mathbf{R}}_i, \tilde{\mathbf{R}}_{i+1}) \\ = -(\Delta\tilde{\mathbf{R}}_i \cdot \mathbf{n}_i) \langle F_i^{\parallel} \rangle = 0, \quad (17)$$

$$W_{i \rightarrow i+1}^{TR}(\tilde{\mathbf{R}}_i, \tilde{\mathbf{R}}_{i+1} + \Delta\tilde{\mathbf{R}}_{i+1}) - W_{i \rightarrow i+1}^{TR}(\tilde{\mathbf{R}}_i, \tilde{\mathbf{R}}_{i+1}) \\ = (\Delta\tilde{\mathbf{R}}_{i+1} \cdot \mathbf{n}_i) \langle F_i^{\parallel} \rangle = \sin(\alpha) \langle F_i^{\parallel} \rangle (\Delta\tilde{\mathbf{R}}_{i+1} \cdot \mathbf{n}_{i \rightarrow i+1}). \quad (18)$$

The rotational component $W_{i+1,i}^{ROT}$ does not contain $\tilde{\mathbf{R}}_i$ at all and thus is unaffected by $\Delta\tilde{\mathbf{R}}_i$. The effect of change in $\tilde{\mathbf{R}}_{i+1}$ is

$$W_{i+1,i}^{ROT}(\tilde{\mathbf{R}}_i, \tilde{\mathbf{R}}_{i+1} + \Delta\tilde{\mathbf{R}}_{i+1}) - W_{i+1,i}^{ROT}(\tilde{\mathbf{R}}_i, \tilde{\mathbf{R}}_{i+1}) \\ = -\alpha \langle F_{i+1}^{\parallel} \rangle (\Delta\tilde{\mathbf{R}}_{i+1} \cdot \mathbf{n}_{i \rightarrow i+1}). \quad (19)$$

Thus both the translational and rotational components of the work have significant dependence on $\tilde{\mathbf{R}}_{i+1}$. The total work $W_{i \rightarrow i+1}$, on the other hand, changes much less with $\tilde{\mathbf{R}}_{i+1}$

$$W_{i \rightarrow i+1}(\tilde{\mathbf{R}}_i, \tilde{\mathbf{R}}_{i+1} + \Delta\tilde{\mathbf{R}}_{i+1}) - W_{i \rightarrow i+1}(\tilde{\mathbf{R}}_i, \tilde{\mathbf{R}}_{i+1}) \\ = (\sin(\alpha) \langle F_i^{\parallel} \rangle - \alpha \langle F_{i+1}^{\parallel} \rangle) (\Delta\tilde{\mathbf{R}}_{i+1} \cdot \mathbf{n}_{i \rightarrow i+1}). \quad (20)$$

The difference in the left brackets of Eq. (20) is expected to be small for nearby hyperplanes and small angles α , since $\sin(\alpha) \approx \alpha$ and $\langle F_i^{\parallel} \rangle \approx \langle F_{i+1}^{\parallel} \rangle$, however, it is nonetheless still nonzero.

A practically important question then is what $\tilde{\mathbf{R}}_i$ should be in order to have numerical $W_{i \rightarrow i+1}$ as accurate as possible. Note that for the stability of the numerical integration itself, a sequence of $\tilde{\mathbf{R}}_i$ should at least form a path that is smooth. At zero temperature the system confined to a hyperplane does not have any kinetic energy to access points with energy higher than a given local minimum. Another way to say it is that at 0 K the probability to find the system at the local minimum is 1, and 0 elsewhere. Then, by choosing $\tilde{\mathbf{R}}_i$ to be at this minimum as well, the force is always applied at the point $\tilde{\mathbf{R}}_i$. Under such circumstances the torque is zero due to the zero arm length [Eq. (11)] and so is the rotational component of the work. Note that at 0 K one could also choose $\tilde{\mathbf{R}}_i$ to be not at the minimum, and then the force is applied off-center and the torque is nonzero.¹⁴ When one uses a minimum energy path (MEP) to define the initial sequence of hyperplanes, the local hyperplane minima will coincide with the MEP points, and so those make good choices for $\tilde{\mathbf{R}}_i$. By MEP we mean a path for which the force is only nonzero in the direction parallel to the path tangent.

Johannesson and Jonsson have suggested to optimize a sequence of hyperplanes along some arbitrarily chosen initial path.¹⁴ This approach yields a hyperplane near the transition state with the translational force and the hyperplane torque both being zero. They have employed $\tilde{\mathbf{R}}_i = \langle \mathbf{R}_i \rangle$ as the reference point for each hyperplane in the sequence. The tangents are being updated in the direction opposite to the torque

vector average, which is $(\langle F_i^{\parallel} \mathbf{R}_i \rangle - \langle F_i^{\parallel} \rangle \tilde{\mathbf{R}}_i)$. Note that in Eq. (12), we evaluated a projection of such torque vector on the specific direction $\mathbf{n}_{i \rightarrow i+1}$ in which the hyperplane was rotated to match the orientation of the other hyperplane.

Ren and E *et al.*^{4,19} have proposed to optimize the entire path at finite temperature—the method referred to as the finite temperature string method. In this approach, an equispaced sequence of hyperplanes is obtained, with tangents \mathbf{n}_i derived from $\langle \mathbf{R}_i \rangle$ via the usual formulas for numerical tangents along a path.²⁰

D. Additional constraints required in molecular systems

Realistic 3D molecules with N atoms have $3N$ degrees of freedom. Out of these, three represent translations of the center of mass, and three represent rotations around it. Note that these translations and rotations of a molecule as a whole in 3D have very little in common with the hyperplane rotations and translations discussed in the context of the free energy integration earlier in this work. The molecular translational degrees of freedom are straightforwardly expressed as linear vectors, while the rotational degrees of freedom can be readily linearized for small rotational angles.²¹ The mass-weighted coordinates are a convenient choice of a coordinate system. Molecular rotations somewhat complicate the use of the $3N$ -dimensional tangents \mathbf{n}_i . Specifically, if the molecular rotations are left unconstrained during the sampling, the molecule can get rearranged by small displacements into a local minimum. The final result of such a change represents a global rotation in a way as to make the tangent \mathbf{n}_i parallel to one of the linearized rotational vectors of this minimized structure.

So in order to make sure that tangent \mathbf{n}_i represents true internal changes within a structure, rotations should be constrained (along with translations). Such a constraint could be either global or local within a chain of configurations. The global one involves the use of Eckart axis conditions^{21–23} with the same fixed structure $\tilde{\mathbf{r}}_a$ for all the structures.¹⁵ Specifically, during the generation of the reaction path one enforces the condition

$$\sum_a m_a \mathbf{r}_a \times \tilde{\mathbf{r}}_a = \mathbf{0}, \quad (21)$$

where $\tilde{\mathbf{r}}_a$ represents atomic positions in some fixed (reference) structure, while \mathbf{r}_a represents atomic positions in any other structure along the MEP. In practice the vector product constraint defined by Eq. (21) can be decomposed into three orthogonal linear constraints of the form

$$\sum_{k=1}^{3N} a_{ak} r_k = 0. \quad (22)$$

Similar constraint equations apply to the three translational constraints, and the reaction path tangent. If all seven linear constraint vectors are made orthogonal, the constraints could be enforced by simply projecting them out sequentially. Otherwise a matrix inversion is needed.^{15,16,24}

An issue with Eq. (21) is that for significant changes in structure \mathbf{r} with respect to the reference one, rotational vec-

tors of $\tilde{\mathbf{r}}$ eliminated from the displacements of structure \mathbf{r} will not be fully aligned with the rotational vectors of structure \mathbf{r} . Then the $(3N-7)$ sampled subspace for structure \mathbf{r} will not represent just the internal degrees of freedom, but a bit of rotation, while a small fraction of the subspace of the internal degrees of freedom will not be sampled due to being constrained. The overall effect of such imperfect rotational constraints will diminish with the increasing number of degrees of freedom.

More interesting, however, is that with local rotational constraints one can in fact make sure that the $(3N-7)$ sampled subspace includes just the internal coordinates only and no rotations. This is achieved by aligning any three consecutive structures \mathbf{r}_1 , \mathbf{r}_2 , and \mathbf{r}_3 in the path to satisfy

$$\mathbf{r}_1 \otimes \mathbf{r}_2 = \mathbf{0}, \quad (23)$$

$$\mathbf{r}_2 \otimes \mathbf{r}_3 = \mathbf{0}, \quad (24)$$

where \otimes denotes a mass-weighted sum of vector products as in Eq. (21). One can construct such a string by using aligning rotation matrices during the string optimization.²⁵ Then the tangents, mainly computed as $[\mathbf{r}_2 - \mathbf{r}_1]$ (with normalization), satisfy both equations

$$(\mathbf{r}_2 - \mathbf{r}_1) \otimes \mathbf{r}_1 = \mathbf{0}, \quad (25)$$

$$(\mathbf{r}_2 - \mathbf{r}_1) \otimes \mathbf{r}_2 = \mathbf{0}, \quad (26)$$

and each structure $\mathbf{r}_i(t)$ could use local rotational constraint $[\otimes \tilde{\mathbf{r}}_i = \mathbf{0}]$, with $\tilde{\mathbf{r}}_i$ taken from the MEP path. Now from structure to structure in the path not only the path tangents but also molecular rotation vectors could be changing orientation (rotating). However, since there should be zero or very small average force (and torque) acting on the molecular rotation constraint vectors, the effect of changing molecular rotation constraints can be neglected. In the following section we will have a numerical example of such an approach.

III. NUMERICAL EXAMPLES

Since our goal is to compute free energy differences of chemical reactions via MD simulations, we will carry out the canonical ensemble sampling in hyperplanes via the MD with a Nose–Hoover thermostat^{26,27} chain.²⁸ It is a well-known by now fact that the simple Nose–Hoover thermostat^{26,27} has poor configurational sampling properties for stiff systems such as a harmonic oscillator.^{27,29} We use Verlet algorithm to integrate the equations of motion, with microiterations for reaching self-consistency between atomic and thermostat velocities.³⁰ The minimum energy path on the surface is obtained via the string method¹¹ with damped dynamics minimization.³¹ The string method is a parameter free approach similar to the nudged elastic band method.¹⁰ The MEP path obtained in such a way represents an equispaced set of configurations which have zero forces perpendicular to the path tangent. The number of thermostats in the Nose–Hoover chain was 10. In line with recommendations of Ref. 28, the first thermostat had the mass of $8gk_B T / (2\pi\nu_{typ})^2$, whereas all the other ones were $8k_B T / (2\pi\nu_{typ})^2$ where g is the number of sampled degrees of

freedom. In the following, we set k_B to 1, and express temperature T in units of the energy. In both examples, we have used 513 replicas along the path including the first and the last points.

The harmonic approximation for the free energy difference between any two points i and j on the path is

$$\Delta A_{i,j}^H = \Delta V_{i,j}^{MEP} - k_B T \ln \left(\frac{\prod_{k=1}^d \nu_{i,k}}{\prod_{k=1}^d \nu_{j,k}} \right), \quad (27)$$

where $\Delta V_{i,j} = V(\tilde{\mathbf{R}}_j^{MEP}) - V(\tilde{\mathbf{R}}_i^{MEP})$. The product $\prod_{k=1}^d$ runs over the frequencies ν_k of all the degrees of freedom accessible to the MD sampling, i.e., those in the hyperplane. To compute frequencies ν_k , we analytically calculated the full Hessian and then projected it onto a smaller subspace from which all the constraint vectors were excluded. The eigenvalues E_k of the projected Hessian can be converted into frequencies via $\nu_k = \sqrt{E_k} / (2\pi)$. The projected out constraints are identical to the ones we use during the MD runs, so our numerical FEP is directly comparable to the harmonic one.

The free energy difference for the same sequence of hyperplanes is also evaluated via the constraint force and hyperplane torque from our MD simulation

$$\Delta A_{i,j}^{MD} = \sum_{l=i}^{j-1} \bar{W}_{l \rightarrow l+1}, \quad (28)$$

where $\bar{W}_{l \rightarrow l+1}$ was defined in Eq. (16).

To facilitate detailed comparisons between the harmonic and numerical FEP, for any two points on the path we define a new quantity ΔM ,

$$\Delta M_{i,j} = \frac{\Delta A_{i,j} - \Delta V_{i,j}^{MEP}}{k_B T}. \quad (29)$$

According to the harmonic approximation [Eq. (27)], harmonic $\Delta M_{i,j}^H$ is independent of the temperature,

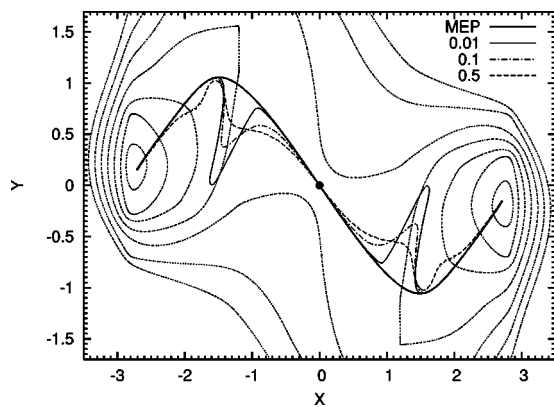
$$\Delta M_{i,j}^H = - \ln \left(\frac{\prod_{k=1}^d \nu_{i,k}}{\prod_{k=1}^d \nu_{j,k}} \right). \quad (30)$$

Note that this logarithm of the frequencies' ratio is often encountered in the context of the transition state theory.¹ We can further split $\Delta M_{i,j}$ into translational and rotational contributions. Since the potential energy differences are purely due to the translational component, the meaningful definitions are

$$\Delta M_{i,j}^{TR} = \frac{\Delta A_{i,j}^{TR} - \Delta V_{i,j}^{MEP}}{k_B T}, \quad (31)$$

$$\Delta M_{i,j}^{ROT} = \frac{\Delta A_{i,j}^{ROT}}{k_B T}. \quad (32)$$

The ΔM 's allow one to see more easily the effects of other minima in the hyperplane as well as anharmonicity on the MD results. Otherwise the free energy profile can be dominated by the potential energy differences $\Delta V_{i,j}$ and the relatively small temperature effects can be overlooked. In addition, highly accurate and sensitive ΔM 's much more clearly illustrate the importance of the rotational contribution.

FIG. 3. Minimum energy and thermally averaged paths at different T s.

A. Model 2D potential

Our first example is a particle with mass 1 in a two-dimensional potential (same as in Ref. 15),

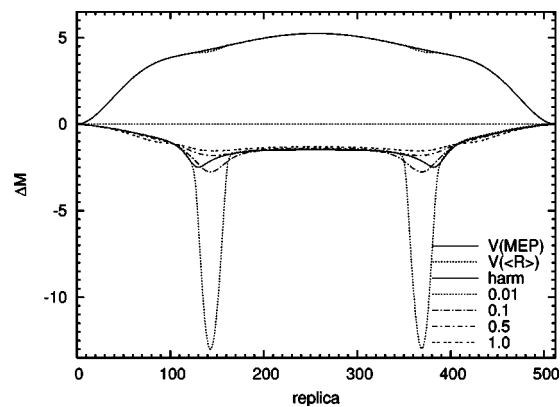
$$V(x,y) = 0.06(x^2 + y^2)^2 + xy - 9e^{-(x-3)^2-y^2} - 9e^{-(x+3)^2-y^2}. \quad (33)$$

This potential has minima at $(\mp 2.7127, \pm 0.1509)$ with the energy of -5.2405 units, whereas the saddle point is at $(0,0)$ with the energy of -0.0022 units (Fig. 3). As mentioned earlier, the MEP path was computed via the string method starting from a linearly interpolated path. The highest frequency in the direction orthogonal to the path is at the minima, with $\nu = 0.68856$. The MD time step was set to $1/100$ th of the characteristic period $1/\nu$. After the initial equilibration for 40 000 steps, the MD simulation was carried out for 8×10^6 steps. The care was taken to avoid finite precision issues by splitting the accumulated averages into pieces. The tangent constraint was maintained via a Lagrange multiplier,²⁴ which in this case is simply the negative of the total force projection on the hyperplane tangent. The harmonic ΔA^\ddagger for the transition state at $(0,0)$ is

$$\Delta A^\ddagger = 5.2383 - 1.4824T. \quad (34)$$

This expression is similar to the one in Ref. 15, with minor differences perhaps due to the slightly different tangent directions at the minimum.

An interesting feature of this potential is that some points along the minimum energy path represent not the global but a local minimum in the respective hyperplane. Then, the probability to find the system is higher at the global

FIG. 4. ΔV_k^{MEP} profile (upper curve) and ΔM at different T s.

minimum. The plot of the original minimum energy path and the averages $\langle \mathbf{R}_i \rangle$ for several different T (Fig. 3) emphasizes this observation.

Comparing harmonic and numerical $\Delta M_k \equiv \Delta M_{0,j}$ (Fig. 4), one can see that at the saddle point these two sets of computed values match quite well at lower temperatures. For the hyperplanes with two minima (Fig. 4, around replica 140), however, ΔM_k^{MD} deviates significantly from the harmonic predictions since then due to a lower minimum an always finite $(\Delta A_{0,j} - \Delta V_{0,j})$ gets divided by whatever small $k_B T$. There is a slight visible energy reduction in this region of the path as computed by using the thermally averaged positions (upper curves in Fig. 4). The splitting of ΔM_k^{MD} into rotational and translational components depends on the reference path employed (Table I and Fig. 5), however, despite very significant redistribution between the two components the total integrated values are very similar. Note that if we simply ignored the rotational component, the obtained ΔM_k^{MD} (and likewise FEP) would be incorrect.

B. A seven-atom Lennard-Jones cluster

The rearrangement of this two-dimensional seven-atom Lennard-Jones (LJ) cluster is investigated in several papers.^{11,32,33} The LJ potential has the standard form

$$V = \sum_{i < j} 4\epsilon \left[\left(\frac{\sigma}{r_{ij}} \right)^{12} - \left(\frac{\sigma}{r_{ij}} \right)^6 \right]. \quad (35)$$

The distance between the particles is r_{ij} , while ϵ and σ are set to 1 (LJ units). The energy for the optimized geometry shown in Fig. 6 is -12.5349 . The question of interest is the

TABLE I. Free energy difference between the minimum and the transition state. The translational and rotational components for two different reference paths are shown. $\Delta A^{\ddagger,H}$ is the harmonic approximation estimate. ΔV^\ddagger is 5.2383.

T	Reference path ($\tilde{\mathbf{R}}_i^{MEP}$)			Reference path ($\langle \mathbf{R}_i \rangle$)				
	ΔA^\ddagger	ΔA_{TR-V}^\ddagger	ΔA_{ROT}^\ddagger	ΔA^\ddagger	ΔA_{TR-V}^\ddagger	ΔA_{ROT}^\ddagger	$\Delta A^{\ddagger,H}$	$\Delta A^{\ddagger,a}$
0.01	5.2238	0.9125	-0.9271	5.2259	0.0363	-0.0487	5.2235	5.223
0.1	5.0919	0.5829	-0.7293	5.0923	0.1688	-0.3149	5.0901	5.092
0.5	4.5404	0.2011	-0.8991	4.5405	-0.1220	-0.5758	4.4971	4.538
1.0	3.9210	-0.6047	-0.7125	3.9210	-0.9608	-0.3565	3.7559	3.933

^aReference 15.

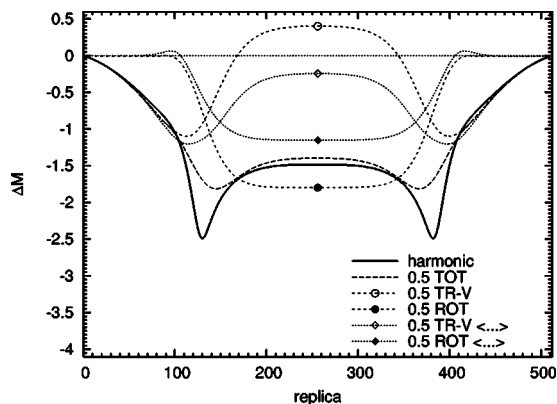


FIG. 5. Translational (TR-V) and rotational (ROT) contributions to ΔM at $T=0.5$ using the minimum energy and thermally averaged paths as $\tilde{\mathbf{R}}_i$.

migration of the center atom to the outer shell of the cluster. One of low activation energy mechanisms for such a rearrangement can be viewed as a rotation of a three-atom group within the cluster (Fig. 6).^{32,33} The intermediate structures relax accordingly in order to be at the valley along the path (i.e., zero force in all directions perpendicular to the path). The profile obtained via the string method has two intermediate minima and three maxima (upper curve in Fig. 7).

The total number of degrees of freedom in this system confined to the xy plane is $2 \times 7 = 14$, out of which two represent translations, and one represents rotation. Including the hyperplane tangent constraint, we end up with the total of four linear constraints, and remaining ten sampled degrees of freedom. During the MD we enforce these two translational, one rotational, and one hyperplane tangent constraints by utilizing Eq. (22).

Figure 7 contains two harmonic ΔM_k approximations where the projected out (constrained in MD) degrees of freedom either were determined by the local or by the global constraint as discussed in Sec. II D. For the ΔM_{global} curve it is quite noticeable that the farther away the structure is located from the central transition state used as the string-wide constraint, the more the ΔM_{global} curve deviates from the ΔM which employed the local rotational constraints. We also want to mention that local constraints are fully consistent

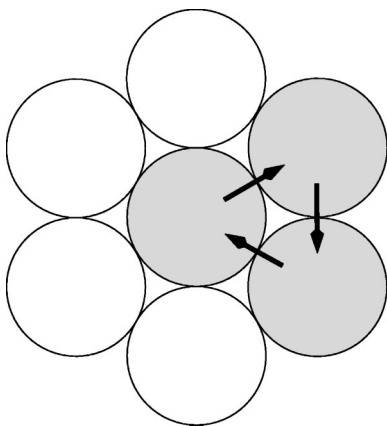


FIG. 6. A two-dimensional LJ cluster.

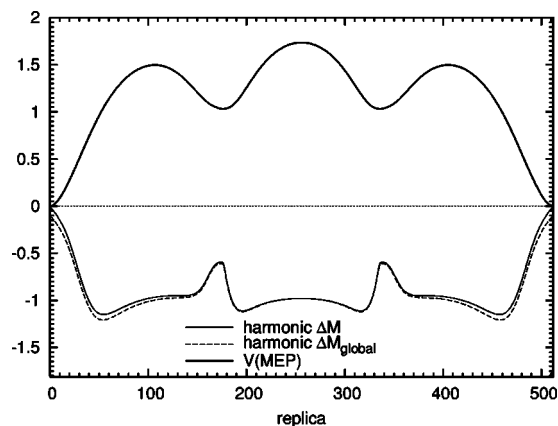


FIG. 7. ΔV_k^{MEP} profile (upper curve) and two harmonic ΔM 's. The curve labeled as ΔM used local rotational constraints for each replica along the string. The curve ΔM_{global} was generated by using the central transition state structure as a constraint for all of the replicas. Both ΔM 's curves are shifted by the same constant, and coincide in the middle where the local and global constraints of the two calculations are the same.

with the way that the usual harmonic frequencies are computed by projecting out translations, rotations, and the force vector if it is nonzero.

The MD simulation was carried out for 8×10^6 time steps with each step being 1/100th of the characteristic period $1/\nu_{\text{typ}}$. The mass of each atom was set to 1. The $\nu_{\text{typ}} = 1.701$ which is the frequency of two bound LJ atoms at the minimum. As one can see from Fig. 8, ΔM_k^{MD} stays relatively close to the harmonic curve for the entire string. We did try several different temperatures, and all numerically computed ΔM_k curves looked very much the same. At sufficiently high thermal energy per structure ($T > 0.01$, not shown), extensive rearrangements start to occur in the hyperplanes.

Again, the individual translational and rotational contributions to the numerical ΔM_k (Fig. 8) with $\tilde{\mathbf{R}}_i = \tilde{\mathbf{R}}_i^{\text{MEP}}$ are of similar magnitude. Simply ignoring the rotational contribution to the ΔM_k^{MD} does get a curve that has the general shape of the harmonic ΔM^H , but unfortunately, it is not a correct one. We also computed the numerical ΔM_k for the string where the central transition state structure was used as the global constraint (not shown). In this case, we could again match the corresponding harmonic $\Delta M_{\text{global}}^H$ curve with the one from the MD.

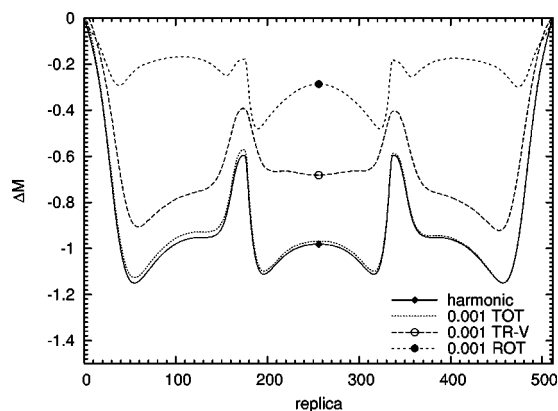


FIG. 8. TR-V and ROT contributions to ΔM at $T=0.001$ using the minimum energy path as $\tilde{\mathbf{R}}_i$. Individual rotational constraint was used for each replica.

IV. CONCLUSIONS

In summary, we have described a convenient computational approach for evaluation of the FEP along some discretized path defined as a sequence of hyperplanes. A hyperplane is fully specified by any its point, and a tangent vector. A suitable path can be obtained by any of the methods such as the intrinsic reaction path,⁹ nudged elastic band,¹⁰ or string method.^{11,12} Sampling along such a path is especially appropriate for chemical reactions where the reactants and products are connected via a single low energy tube, so the neighborhood of the minimum energy path is a good representation of the configuration space region through which pass almost all reactive trajectories.

The FEP is obtained as an integral of two components [Eq. (6)]. The translational component of the free energy is computed by integrating the hyperplane constraint force [Eq. (7)]. The rotational component is evaluated via the hyperplane torque [Eq. (13)]. Both ingredients—the constraint force and the hyperplane torque—are evaluated on each hyperplane independently by computing two simple averages. This is in contrast to the method of Neria *et al.*,¹⁵ where the change in free energy is computed by considering two neighboring hyperplanes at once. The differential form of our expressions is the same as the one utilized by Jonsson and co-workers.^{13,14} The accuracy of our integration procedure can be improved systematically by inserting hyperplanes in between, and the additional sampling only needs to be done on these added hyperplanes while keeping the averages for existing ones.

Our integration procedure utilizes a set of reference points defining a point of rotation on each hyperplane and these points can be chosen before or after the sampling takes place. A shift in the reference points significantly redistributes the FEP contributions between the translational and rotational components. In contrast, the total of the two components is affected to a much lesser extent.

The validity of the presented method is demonstrated on two examples, a simple 2D potential, and seven-atom Lennard-Jones cluster in two dimensions. In each case, we compared the numerical FEP with the harmonic approximation estimates. Our results for the 2D potential are also verified by the data available in the literature. We emphasize the fact that the evaluation of the rotational contribution is vital for computing correct FEPs.

ACKNOWLEDGMENT

This material is based upon work supported in part by the U.S. Army Research Office Multidisciplinary University Research Initiative (ARO/MURI) under Grant No. W911NF-04-1-0170. The work was also partially supported by NSF Award No. CHE-0121432.

- ¹J. I. Steinfeld, J. S. Francisco, and W. L. Hase, *Chemical Kinetics and Dynamics*, 2nd ed. (Prentice-Hall, Upper Saddle River, NJ, 1999).
- ²R. Car and M. Parrinello, *Phys. Rev. Lett.* **55**, 2471 (1985).
- ³E. A. Carter, G. Ciccotti, J. T. Hynes, and R. Kapral, *Chem. Phys. Lett.* **156**, 472 (1989).
- ⁴Weinan E and E. Vanden-Eijnden, in *Multiscale Modeling and Simulation*, Lecture Notes in Computational Science and Engineering, Vol. 39, edited by S. Attinger and P. Koumoutsakos (Springer-Verlag, Berlin, 2004).
- ⁵C. H. Bennett, in *Algorithms for Chemical Computation*, ACS Symposium Series No. 46, edited by R. E. Christofferson (American Chemical Society, Washington, DC, 1977), p. 63.
- ⁶D. Chandler, *J. Chem. Phys.* **68**, 2959 (1978).
- ⁷W. K. den Otter and W. J. Briels, *J. Chem. Phys.* **109**, 4139 (1998).
- ⁸M. Sprik and G. Ciccotti, *J. Chem. Phys.* **109**, 7737 (1998).
- ⁹K. Fukui, *Acc. Chem. Res.* **14**, 363 (1981).
- ¹⁰H. Jonsson, G. Mills, and K. Jacobson, in *Classical and Quantum Dynamics in Condensed Phase Simulations*, edited by B. J. Berne, G. Ciccotti and D. F. Coker (World Scientific, Singapore, 1998).
- ¹¹Weinan E, W. Ren, and E. Vanden-Eijnden, *Phys. Rev. B* **66**, 052301 (2002).
- ¹²W. Quapp, *J. Comput. Chem.* **25**, 1277 (2004).
- ¹³G. K. Schenter, G. Mills, and H. Jonsson, *J. Chem. Phys.* **101**, 8964 (1994).
- ¹⁴G. H. Johansson and H. Jonsson, *J. Chem. Phys.* **115**, 9644 (2001).
- ¹⁵E. Neria, S. Fischer, and M. Karplus, *J. Chem. Phys.* **105**, 1902 (1996).
- ¹⁶R. Elber, *J. Chem. Phys.* **93**, 4312 (1990).
- ¹⁷W. K. den Otter, *J. Chem. Phys.* **112**, 7283 (2000).
- ¹⁸A. Michalak and T. Ziegler, *J. Phys. Chem. A* **105**, 4333 (2001).
- ¹⁹W. Ren and W. E (unpublished).
- ²⁰G. Henkelman and H. Jonsson, *J. Chem. Phys.* **113**, 9978 (2000).
- ²¹C. Eckart, *Phys. Rev.* **47**, 552 (1935).
- ²²H. M. Pickett and H. L. Strauss, *J. Am. Chem. Soc.* **92**, 7281 (1970).
- ²³A. Y. Dymarsky and K. N. Kudin, *J. Chem. Phys.* (in press).
- ²⁴J. P. Ryckaert, G. Ciccotti, and H. J. C. Berendsen, *J. Comput. Phys.* **23**, 327 (1977).
- ²⁵K. N. Kudin and R. Car (unpublished).
- ²⁶S. Nose, *J. Chem. Phys.* **81**, 511 (1984).
- ²⁷W. G. Hoover, *Phys. Rev. A* **31**, 1695 (1985).
- ²⁸G. J. Martyna, M. L. Klein, and M. Tuckerman, *J. Chem. Phys.* **97**, 2635 (1992).
- ²⁹S. Toxvaerd and O. H. Olson, *Ber. Bunsenges. Phys. Chem.* **94**, 274 (1990).
- ³⁰G. Ciccotti and J.-P. Ryckaert, *Comput. Phys. Rep.* **4**, 345 (1986).
- ³¹Y. Kanai, A. Tilocca, A. Selloni, and R. Car, *J. Chem. Phys.* **121**, 3359 (2004).
- ³²C. Dellago, P. G. Bolhuis, and D. Chandler, *J. Chem. Phys.* **108**, 9236 (1998).
- ³³D. J. Wales, *Mol. Phys.* **100**, 3285 (2002).